Gold nanoparticle biodissolution by a freshwater macrophyte and its associated microbiome

Astrid Avellan, Marie Simonin, Eric Mcgivney, Nathan Bossa, Eleanor Spielman-Sun, Jennifer Rocca, Emily S Bernhardt, Nicholas K Geitner, Jason M Unrine, Mark R. Wiesner, et al.

ARTICLES
https://doi.org/10.1038/s41565-018-0231-y
nature nanotechnology

Gold nanoparticle biodissolution by a freshwater macrophyte and its associated microbiome

Astrid Avellan[1,2], Marie Simonin[1,3], Eric McGivney[1,2], Nathan Bossa[1,4], Eleanor Spielman-Sun[1,2], Jennifer D. Rocca[3], Emily S. Bernhardt[1,3], Nicholas K. Geitner[1,4], Jason M. Unrine[1,5], Mark R. Wiesner[1,4] and Gregory V. Lowry[1,2*]

Predicting nanoparticle fate in aquatic environments requires mimicking of ecosystem complexity to observe the geochemical processes affecting their behaviour. Here, 12 nm Au nanoparticles were added weekly to large-scale freshwater wetland mesocosms. After six months, ~70% of Au was associated with the macrophyte *Egeria densa*, where, despite the thermodynamic stability of Au^0 in water, the pristine Au^0 nanoparticles were fully oxidized and complexed to cyanide, hydroxyls or thiol ligands. Extracted biofilms growing on *E. densa* leaves were shown to dissolve Au nanoparticles within days. The Au biodissolution rate was highest for the biofilm with the lowest prevalence of metal-resistant taxa but the highest ability to release cyanide, known to promote Au^0 oxidation and complexation. Macrophytes and the associated microbiome thus form a biologically active system that can be a major sink for nanoparticle accumulation and transformations. Nanoparticle biotransformation in these compartments should not be ignored, even for nanoparticles commonly considered to be stable in the environment.

Understanding the reactivity of nanoparticles in the environment is essential for unbiased assessments of their fate and impacts. To accurately measure nanoparticle transformation rates, determine the mechanisms of transformation, and identify the environmental compartments where transformations occur, reactivity assessments of nanoparticles should be done in ways that capture their complex and dynamic natural behaviour[1]. Mesocosms mimicking emergent freshwater wetlands are good tools for elucidating nanoparticle fate in complex aquatic systems[2–5] because they include submerged and unsubmerged zones and host a large diversity of organisms. Using long-term low-nanoparticle-dose exposure scenarios in these mesocosms will also reveal the natural biogeochemical processes driven by seasonal effects that may affect the fate of nanoparticles[5].

Nanoparticles have unique properties that can lead to specific benefits and impacts[6,7], and studying nanoparticle-specific behaviour in aquatic environments requires the use of nano-metallic tracers that are thermodynamically stable under environmental variations. For example, gold nanoparticles (Au-NPs) are often used as inert metallic tracers to follow specific nanoparticle behaviour in aquatic environments[8–20], because they are relatively unreactive in abiotic water. Indeed, the standard oxidation potentials of Au^0 to Au^+ and Au^{3+} exceed that of water (equations (1), (2) and (3)), making the formation of ionic Au in abiotic water thermodynamically unfavourable[21]:

$$Au^0(s) \rightarrow Au^+(aq) + e^- \quad E^0 = -1.68\ V \tag{1}$$

$$Au^0(s) \rightarrow Au^{3+}(aq) + 3e^- \quad E^0 = -1.5\ V \tag{2}$$

$$2H_2O(l) \rightarrow O_2(g) + 4H^+(aq) + 4e^- \quad E^0 = -1.23\ V \tag{3}$$

However, the assumption of Au-NP stability could be incorrect in biologically active media because (1) it has been demonstrated that the oxidative dissolution of metallic gold can occur in biologically active soils[22–24] (as described later), and (2) the inherent increased reactivity of nanosized particles[6] could further enhance biodissolution rates. Two studies assessing the fate of Au-NPs in aquatic environments have hypothesized that Au-NPs could dissolve[18] or undergo surface oxidation[19], but most studies do not assess Au-NP transformation in their experiments. Few studies have demonstrated the absence of Au-NP dissolution under particular conditions, in abiotic aqueous medium[20], or confirming the absence of oxidized Au in vivo[25–27]. However, no studies have assessed the role of (micro)organisms and their biomolecules on Au-NP transformations in a biologically active complex aquatic system. Thus, knowledge of how important these processes are in driving nanoparticle fate in aquatic environments is sparse.

The relative stability of Au-NPs against transformation may depend on the conditions that have been used to study their fate; that is, using relatively high concentrations of Au-NPs in abiotic systems or in systems with limited biological complexity, which may limit reactivity. As for other metallic nanoparticles, not accounting for the biotransformation of Au-NPs can lead to the misinterpretation of fate processes of non-dissolving nanoparticles by incorrectly assigning observations of metal uptake and transport to specific particulate behaviour rather than ionic species. So far, the fate of metallic nanoparticles has been predicted using models[28–30] that often only account for strictly abiotic nanoparticle transformations. It can also lead to confusion about mechanisms of toxicity by attributing toxicity to specific nanoparticle impacts rather than the released ions known to affect the functioning of the biological system[31].

The biotransformation of Au-NPs in a biologically active aquatic environment is possible. Soil microorganisms could solubilize Au^0 via bio-oxidation and stabilization through complexation[22]. These

[1]Center for the Environmental Implications of NanoTechnology (CEINT), Durham, NC, USA. [2]Department of Civil and Environmental Engineering, Carnegie Mellon University, Pittsburgh, PA, USA. [3]Department of Biology, Duke University, Durham, NC, USA. [4]Civil & Environmental Engineering, Duke University, Durham, NC, USA. [5]Department of Plant and Soil Sciences, University of Kentucky, Lexington, KY, USA. *e-mail: glowry@andrew.cmu.edu

processes could happen with the emission of different ligands. Some soil bacteria can generate thiosulfates[32], which can lead (in oxic environments) to Au oxidation and complexation[33]. Cyanide is well known for its ability to oxidize and complex Au^0 and can be released by plants, fungi and soil bacteria[34]. The reactivity of bulk Au^0 in soils and sediments has been investigated, and bio-driven geochemical models of Au cycling in soils have been proposed[22,23]. However, though solubilization of Au^0 in soil or sediments has been correlated with the presence of microorganisms[35], or demonstrated using isolated strains of cyanogenic soil bacteria cultivated under cyanide-forming condition[36,37], there is no understanding of the mechanisms of transformation of Au species in biologically active compartments of the water column.

One important biologically active sink for metals in aquatic environments comprises aquatic vascular plants (macrophytes) and their associated microbiome. Freshwater wetlands are often dominated by one macrophyte species[38] that, by virtue of its high surface area, plays a dominant role in metal uptake, transformation, storage and thus entry of contaminants into the aquatic food webs[39]. In particular, macrophytes in wetland mesocosms have been found to have an affected metabolism under Au- and Cu-based nanoparticle exposure[5] and form a significant sink for the accumulation of both pristine and transformed Cu- and Ag-based nanoparticles[4]. The initial contact between nanoparticles and these macrophytes will be with the surface microbiome of the plant, a matrix of organic and inorganic materials including biologically active microbial biofilms[40]. In the case of Au-NPs, these biofilms could be an important driver for Au-NP biotransformation and fate, because Au from Au-NPs has been found to accumulate in macrophytes[10] and in biofilms[8,9], from where Au species can then be transferred into the food chain[41]. Monitoring Au-NP biotransformations in these important aquatic reservoirs will improve our understanding of Au-NP cycling in aquatic environments, but they can also highlight some biological processes potentially affecting metallic nanoparticles in aquatic environments, including the rate and timescales at which accumulation and biotransformation can play a role in nanoparticle fate, and the organisms driving these processes.

Here, the accumulation and transformations of Au-NPs in macrophytes and associated biofilms were studied at the system level to elucidate the complex fate processes impacting Au-NPs. Low doses of metallic Au-NPs were added weekly to the water column of an aquatic freshwater wetland mesocosm for six months. The majority (~70%) of Au dosed in the mesocosms was found to be associated with the macrophyte *Egeria densa* and the biofilms growing on its shoots. This Au was not metallic, but transformed to oxidized species (Au-hydroxide, Au-cyanide and Au-thiols). The capacity for the biofilms on *E. densa to* perform this oxidation was investigated by exposing them to Au-NPs in vitro. These biofilms were able to dissolve a significant fraction (25–45%) of Au-NPs, and their biodissolution efficiency increased with the presence of bacterial communities less adapted to metallic environments and with a higher capacity to release cyanide.

Au-NP accumulation and biotransformation

Au-NP fate was assessed in large replicated outdoor freshwater wetland mesocosms. The mesocosms were representative of a natural system, including an upland, a transition (periodically flooded) and an aquatic zone, with a large diversity of species and a complex food web (Supplementary Fig. 1). For six months, citrate-coated Au-NPs (~12 nm in diameter; Supplementary Fig. 2) were added weekly into the mesocosms' ($n=3$) water column (~300 l) until a total mass of 500 mg of Au had been added. Three additional non-exposed mesocosms served as controls.

After six months of chronic additions of Au-NPs, the concentration of Au in the water column was only $4.4\pm3.7\,\mu g\,Au\,l^{-1}$, while Au concentrations associated with the macrophyte *E. densa* were

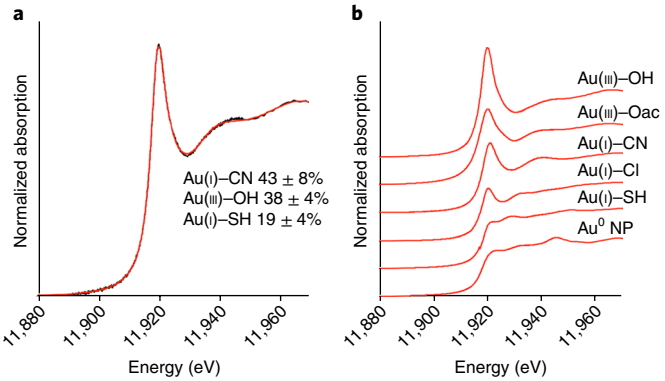

Fig. 1 | Speciation of Au associated to *E. densa* from mesocosms chronically exposed to Au-NPs for six months. a, XANES spectra at the Au–L_{III} edge of young shoots of *E. densa*. Experimental (black line) and calculated (red line) signals are presented as well as the proportion of each reference compound used in the fits. Quality factors resulting from this fit: *R*-factor $=2.3\times10^4$, $\chi^2=0.02$, reduced $\chi^2=4.5\times10^5$. **b**, Reference compounds considered in fitting the experimental spectra. There is no contribution of Au^0 to the sample spectra.

$500\pm32\,mg\,Au\,kg^{-1}$ (dry mass). Au concentrations in the control mesocosms were below the method detection limits (MDLs) in both water and *E. densa* (MDL $=0.7\,\mu g\,Au\,l^{-1}$ in water and $0.2\,mg\,Au\,kg^{-1}$ of dry plants). The macrophyte biomass in the Au-NP-dosed mesocosms after six months was calculated to be 717 ± 89 g (dry mass). Thus, after six months, ~60–80% of the added Au was associated with *E. densa*. This level of accumulation makes the macrophyte the most important sink for Au in this system. Previous mesocosm experiments did not adequately assess the role of macrophytes on metallic nanoparticle fate. A previous study on Au-NPs in an estuarine mesocosm did not contain any submerged macrophytes[8]. Our previous study in a freshwater wetland mesocosm showed that *E. densa* strongly accumulated Ag- and Cu-based nanoparticles[4], but the high doses of nanoparticles used induced detrimental effects on the macrophytes[4,42], which led to low dissolved oxygen concentrations and high dissolved organic carbon[42], probably affecting nanoparticle fate[31].

An X-ray absorption near edge structure (XANES) spectrum of the *E. densa* tissues exposed to Au-NPs for six months was recorded at the Au–L_{III}edge (Fig. 1a), along with reference spectra (Fig. 1b) to determine if any transformation of Au-NPs results from the accumulation by *E. densa* and its associated microbiome. The XANES spectrum indicates that 100% of the Au associated with the plant tissues was oxidized, with no contribution of metallic Au^0 to the signal. Linear combination fitting with Au reference spectra indicated that the Au associated to *E. densa* tissues was complexed with cyanide (43 ± 8%), hydroxide (38 ± 4%) and thiol (19 ± 4%) ligands. To our knowledge, this is the first description of the oxidation of metallic Au in association with an aquatic macrophyte. Giving the pH (9.2 ± 0.6) and the oxic conditions (dissolved oxygen 144 ± 28% saturation) in the mesocosm water dosed with Au-NPs (Supplementary Fig. 3), these Au complexes should be stable[43]. This Au association with *E. densa* is consistent with previous microcosm (laboratory-based) studies that measured elevated Au concentrations ($5–25\,mg\,Au\,kg^{-1}$) in *E. densa* exposed to $250\,\mu g\,Au\text{-}NPs\,l^{-1}$ (refs. [10,44]). This accumulation was attributed to Au-NP surface adsorption onto the plants rather than assimilation (based on transmission electron microscopy (TEM) observations). It is unclear if any Au^0 oxidation had occurred in their system because Au speciation was not determined.

Here, the presence of Au–cyanide complexes is probably due to the release of cyanide by cyanogenic organisms, as investigated later. Dissolution of Au^0 by cyanide is a two-step reaction. Hydrogen

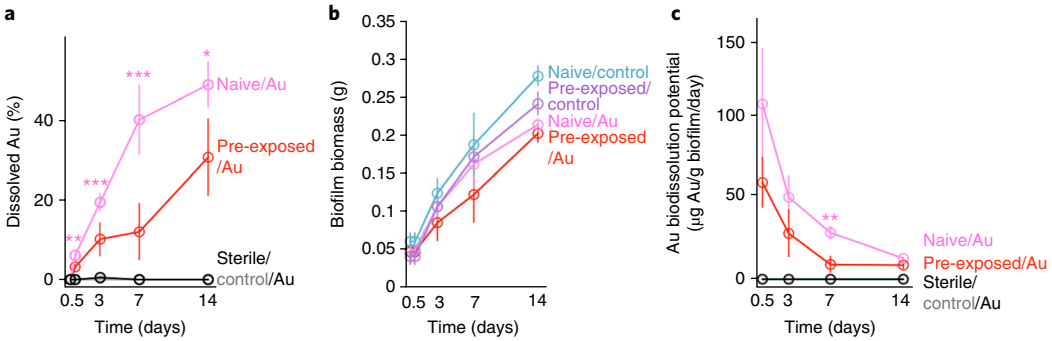

Fig. 2 | Au biodissolution potentials of the naive and the pre-exposed biofilms. a, Biodissolution of Au-NPs during incubation in sterile conditions (sterile/Au), or in the presence of biofilms (naive/Au or pre-exposed/Au) over two weeks. **b**, Biofilm biomass over time of naive or pre-exposed biofilm, unexposed controls or exposed to 70 µg l^{-1} of Au-NPs. **c**, Resulting biodissolution potential of Au-NPs by the biofilms. The dissolved Au fraction in the sterile mesocosm water was below the MDLs. Asterisks indicate significant differences between the conditions: $^{*}P<0.05$, $^{**}P<0.01$, $^{***}P<0.001$. The lower statistical significance ($P<0.06$) of dissolution rate at earlier times is a result of the relatively high variability of the biomass measured in the system.

cyanide (HCN) is a weak acid ($pK_a=9.31$)[45], which dissociates in water to form CN^- and H^+. Oxygen is reduced and hydrogen peroxide is formed as an intermediate product, becoming the oxidizing agent. Au^0 will thus be oxidized, and free cyanide in solution will complex with Au ions to form $Au(CN)_2^-$ (ref. [43]). A summary of these partial reactions is represented in the Elsner reaction:

$$4Au + 8CN^- + O_2 + 2H_2O \rightarrow 4Au(CN)_2^- + 4OH^- \quad (4)$$

The strong complex that is formed between Au^+ and CN^- ($K=10^{39}$)[43] results in a low standard electron potential for Au oxidation and complexation in the presence of cyanide, rendering the formation of $Au(CN)_2^-$ complexes favourable in water[43]:

$$Au(CN)_2^- + e^- \rightarrow Au + 2CN^- \quad E^0 = -0.57\ V \quad (5)$$

Finally, the pH ranges measured in the mesocosms are close to the HCN pK_a, making the cyanation process possible (Supplementary Fig. 3a). The presence of $Au(OH)_3$(s) in this system could be generated from the presence of other oxidizing agents, such as reactive oxygen species (ROS), either oxidizing Au^0 at elevated pH, or from precipitation of $Au(OH)_3$ in oxidative alkaline environments when OH– ligands can outcompete the CN– ligand for Au(III) (ref. [43]). The standard reduction potential of $Au(OH)_3$ to Au is lower at higher pH ($E^0=1.48$ V–0.0591 pH)[21]. Finally, because thiols cannot oxidize Au^0, the presence of Au–thiol compounds could be a result of the displacement of CN ligands by S–R (thiol) groups, leading to the formation of soluble $[RSAuCN]^-$ or $[RS_2Au]^-$ complexes[46]. All these Au transformations are likely to happen in the mesocosm system because the pH was high, so were the dissolved oxygen concentrations during the day (up to 200% saturation) due to macrophyte photosynthesis (Supplementary Fig. 3a,b).

Microbial biofilm composition and gold dissolution capacity

Biofilms were extracted from 25 young shoots of *E. densa* collected from each mesocosm, and tested for their ability to dissolve Au-NPs. Hereon, biofilms will be called 'naive biofilm' if taken from a control mesocosm and 'pre-exposed biofilm' if collected from a mesocosm exposed to Au-NPs for six months. The weight of biofilm extracted represented ~0.1% of the *E. densa* biomass (dry mass). Though the naive biofilm did not contain any Au, pre-exposed biofilm concentrations were 140 ± 60 mg Au kg^{-1} of biofilm (dry mass), which was higher than the surrounding Au concentration in water (~4 µg Au l^{-1}). Previous studies showed a very high bioaccumulation of Au from Au-NPs (60%) by biofilms growing on glass slides in an estuarine mesocosm[8], as well as the potential for trophic transfer of Au-NPs from periphytic biofilms to *Gammarus fossarum* under laboratory conditions[41]. The present results show that epiphytic biofilms in freshwater mesocosms constitute a compartment able to accumulate high concentrations of Au-NPs directly at the surface of aquatic plants.

The naive and pre-exposed biofilms were characterized through 16S rRNA genes sequencing (raw sequence data are provided in the Supplementary Information). Even though pre-exposed and naive biofilms had a similar richness (number of taxa, operational taxonomic units (OTUs)), their community compositions were different (88% of dissimilarity, Supplementary Figs. 4a,b and 5). From the 900 OTUs that are specific to the pre-exposed biofilm, 389 (43%) belonged to OTUs that have been described to be present in metal-impacted environments, or known to have a tolerance to heavy metals. For instance, the pre-exposed biofilm shows an increase in OTUs in the Cytophaga–Flavobacterium group of Bacteroidetes[47], or in the family Nostocaceae of cyanobacteria[48], as well as in the genera *Sulfurospirillum*[49], *Clostridiaceae*[50], *Dechloromonas*[51,52] and *Pseudomonas*[53], the latter also being cyanogenic[23,34]. It is noteworthy that with the samples collected (a composite sample of biofilm from the 25 *E. densa* shoots collected in one mesocosm per treatment), we cannot conclude that these differences were a result of Au-NP exposure, as natural variation could occur. However, they represent differences between the microbial communities that were used as inocula for in vitro experiments to determine the rate, extent and mechanism of Au-NP dissolution, as discussed later. These differences in microbial community composition, especially through an enrichment of metal-tolerant taxa in the pre-exposed biofilm, provide insight into the organisms that are responsible for the later described Au-NP biodissolution observations.

Naive and pre-exposed biofilms were incubated for two days in sterilized mesocosm water and then exposed to Au-NPs (70 µg Au l^{-1}) along with biotic and sterile controls (four replicates each; Supplementary Table 1). Total and dissolved Au concentrations in water were measured after 0, 0.5, 3, 7 and 14 days of incubation. After two weeks, both the naive and pre-exposed biofilms dissolved large fractions of Au-NPs (45 and 25%, respectively) after 14 days of incubation (Fig. 2a). This high Au dissolution rate in vitro suggests that the oxidized Au detected in association with *E. densa* tissues probably resulted in major part from a local dissolution of Au mediated by the biofilm present on the macrophyte.

These results also suggest a difference in biofilm dissolution capacities associated with initial differences in the composition of the biofilms, because no significant differences in biofilm biomass were observed under the different conditions (Fig. 2b). Initially, the

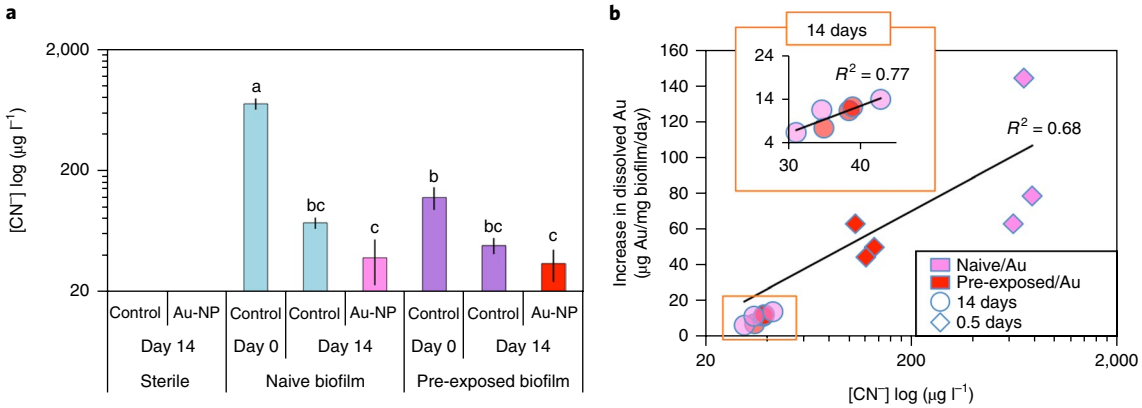

Fig. 3 | Cyanide emission by biofilms and Au biodissolution. a, Concentration of cyanide ions (CN^-) in the dissolved fraction of the samples (MDL of 25 µg l^{-1}). Different letters indicate significantly different groups between treatments ($\alpha = 0.05$; two-way analysis of variance (ANOVA) followed by Tukey's honest significant difference (HSD) test). **b**, Pearson correlation between cyanide concentration and Au biodissolution rates for naive (pink) or pre-exposed (red) biofilms incubated with Au-NPs for 0.5 days (diamonds) or 14 days (circles, magnified in orange inset). *P* values of the Pearson correlations were <0.002.

Au-NP dissolution potential in the pre-exposed biofilm treatments was lower than in the naive biofilms (Fig. 3b). However, by the end of the experiments, the two biofilms reached a similar dissolution potential (~10 µg of Au per g of pre-exposed biofilm per day). This relatively rapid decrease of the Au biodissolution potential suggests that (1) Au-NPs and/or their transformed species modify the efficiency of the biofilm responsible for Au-NP dissolution, for example via microorganisms selection, and/or (2) that exposures to Au-NPs lead to the release of biomolecules that can either bind or precipitate ionic Au, and/or reduce it back to insoluble species[23,24].

Biofilm release of cyanide and gold complexation

The main driver of Au metal oxidative biodissolution in a low-salinity aquatic oxic environment is likely to be through Au oxidation and complexation with cyanide (as described earlier), which can be emitted by microorganisms as a secondary metabolite[24,34]. The concentration of free cyanide (both HCN and CN^-) released before Au-NP addition by the naive biofilm (~700 µg l^{-1}) was significantly higher than the release by the pre-exposed biofilm (~120 µg l^{-1}) (day 0, in vitro incubation, Fig. 3). This was probably due to a difference in composition of the pre-exposed biofilm communities and their potential to release[34] or degrade[54] cyanide. Indeed, OTUs affiliated to taxa able to degrade cyanide were more abundant in the pre-exposed biofilm, such as the genera *Pseudomonas* (pre-exposed: 716 versus naive 391 OTUs) or *Bacillus* (pre-exposed: 3 versus naive 0 OTUs)[55]. In contrast, some OTUs of families presenting taxa capable of cyanide release were more abundant in the naive biofilm, such as Neisseriaceae (naive: 452 versus pre-exposed: 61 OTUs) or Cyanobacteriaceae (naive: 115 versus pre-exposed 1 OTU)[55]. The higher concentration of free cyanide in solutions of the naive biofilm before Au-NP exposure could be the result of a detoxification mechanism[34], and could explain the overall higher initial Au-NPs biodissolution rate induced by the naive biofilms (Fig. 2a).

After 14 days, the concentration of free cyanide in solution significantly decreased for both biofilms. This could be due to the formation of $Au(CN)_2^-$ complexes, which will reduce the overall CN^- concentration, $Au(CN)_2^-$ being not detectable by the probe. The pH also decreased over time (Supplementary Fig. 6), probably leading to the formation of volatile HCN ($pK_a = 9.3$)[45]. Microorganisms also probably played a role in the cyanide concentration decrease, because free cyanide could be use as a nitrogen source by the biofilms[54]. Finally, the overall cyanide emission could decrease as the biofilm production reduced and the community composition changed over time.

It is very likely that the formation of $Au(CN)_2^-$ is one of the major mechanisms inducing Au-NP biodissolution by the biofilm. Indeed, concentrations of free cyanide and dissolved Au concentrations are consistent with a 2:1 CN:dissolved Au ratio required to form $Au(CN)_2^-$ complexes. Furthermore, the measured free cyanide was positively correlated to the Au biodissolution potential ($R^2 = 0.68$, $P = 0.002$), which was even stronger after 14 days ($R^2 = 0.77$, $P < 0.001$). $Au(CN)_2^-$ complexes were detected in the presence of the naive biofilm but not the pre-exposed biofilm (Supplementary Fig. 7). This result is consistent with the dissolution potential being highest for the naive biofilm. In the case of the pre-exposed biofilm, the fact that both a lower level of cyanide at day 0 (Fig. 3) and a lower dissolution potential (Fig. 2) was observed could explain why $Au(CN)_2^-$ was not detected in this sample. Finally, the biofilm growth induced a water pH decrease of 0.3–0.5 pH units over the time of the experiment (Supplementary Fig. 6), certainly lowering the amount of free cyanide in solution and thus decreasing the formation of $Au(CN)_2^-$.

Finally, the earlier description of the presence of cyanide, hydroxyls and thiols complexed to Au in association with *E. densa* is probably a result of Au biodissolution by the biofilms growing on the macrophyte, through cyanide complexation and further stabilization. Simultaneously, precipitation of hydroxide phases and reactions with thiolized molecules could also be a microorganism-driven process, even though *E. densa* very probably plays a role in further transforming the oxidized Au species. These subsequent biotransformations could happen through Au adsorption or uptake[10,44], the release of ROS that could lead to $Au(OH)_3$ precipitation[45], or the emission of dissolved organics (potentially presenting thiol groups) that could reduce[56], precipitate[57] and/or further stabilize[31] the oxidized Au.

Conclusions

Contrary to previous assumptions about the stability of Au-NPs in oxic freshwater environments, this study clearly demonstrates that low doses of Au-NPs added into a complex and biologically active freshwater wetland environment are oxidized and complexed by biofilms growing on macrophytes. This is the result of series of occurrences, including the fact that *E. densa* and its associated biofilm are an important sink for nanoparticles, and that the associated biofilm produces cyanide in sufficient quantity to promote Au-NP oxidative dissolution. The formation of a mixture of oxidized gold complexed with cyanide, hydroxyl or thiol groups was probably due to several factors, as the presence of biofilms and

plant biomolecule emission are impacted by seasonal changes. The Au biotransformation would probably also not have been observed if the experiment had been done using higher nanoparticle doses, for shorter times, in a system with less biological complexity, or if macrophytes had not been included in the study and carefully examined. Furthermore, hydroxide and cyanide ligands responsible for Au-NP biotransformation can also bind to many other metals, making these biologically active compartments, and major sinks for NPs, potentially significant drivers of the fate of a broad range of metallic nanoparticles. Additional explorations are required to elucidate their role in metal nanoparticle geochemical cycling in aquatic environments. Finally, many (micro)organisms can release strong chelators, biomacromolecules, dissolved organic matter or amino acids that could also modify nanoparticle fate. Future research should focus on assessing, quantifying and modelling where, how and at what rates these types of biotransformation process will occur.

Methods

Methods, including statements of data availability and any associated accession codes and references, are available at https://doi.org/10.1038/s41565-018-0231-y.

Received: 13 January 2018; Accepted: 13 July 2018;
Published online: 13 August 2018

References

1. Schirmer, K. & Auffan, M. Nanotoxicology in the environment. *Environ. Sci. Nano* **2**, 561–563 (2015).
2. Lowry, G. V. et al. Long-term transformation and fate of manufactured Ag nanoparticles in a simulated large scale freshwater emergent wetland. *Environ. Sci. Technol.* **46**, 7027–7036 (2012).
3. Auffan, M. et al. An adaptable mesocosm platform for performing integrated assessments of nanomaterial risk in complex environmental systems. *Sci. Rep.* **4**, 5608 (2014).
4. Stegemeier, J. P., Avellan, A. & Lowry, G. V. Effect of initial speciation of copper- and silver-based nanoparticles on their long-term fate and phytoavailability in freshwater wetland mesocosms. *Environ. Sci. Technol.* **51**, 12114–12122 (2017).
5. Simonin, M. et al. Engineered nanoparticles interact with nutrients to intensify eutrophication in a wetland ecosystem experiment. *Ecol. Appl.* https://doi.org/10.1002/eap.1742 (2018).
6. Auffan, M. et al. Towards a definition of inorganic nanoparticles from an environmental, health and safety perspective. *Nat. Nanotech.* **4**, 634–641 (2009).
7. Khan, I., Saeed, K. & Khan, I. Nanoparticles: Properties, applications and toxicities. *Arab. J. Chem.* (in the press).
8. Ferry, J. L. et al. Transfer of gold nanoparticles from the water column to the estuarine food web. *Nat. Nanotech.* **4**, 441–444 (2009).
9. Burns, J. M. et al. Surface charge controls the fate of Au nanorods in saline estuaries. *Environ. Sci. Technol.* **47**, 12844–12851 (2013).
10. Glenn, J. B. & Klaine, S. J. Abiotic and biotic factors that influence the bioavailability of gold nanoparticles to aquatic macrophytes. *Environ. Sci. Technol.* **47**, 10223–10230 (2013).
11. Wray, A. T. & Klaine, S. J. Modeling the influence of physicochemical properties on gold nanoparticle uptake and elimination by *Daphnia magna*. *Environ. Toxicol. Chem.* **34**, 860–872 (2015).
12. Lovern, S. B., Owen, H. A. & Klaper, R. Electron microscopy of gold nanoparticle intake in the gut of *Daphnia magna*. *Nanotoxicology* **2**, 43–48 (2008).
13. Ferreira, P., Fonte, E., Soares, M. E., Carvalho, F. & Guilhermino, L. Effects of multi-stressors on juveniles of the marine fish *Pomatoschistus microps*: gold nanoparticles, microplastics and temperature. *Aquat. Toxicol.* **170**, 89–103 (2016).
14. Khan, F. R. et al. In vivo retention of ingested Au NPs by *Daphnia magna*: no evidence for trans-epithelial alimentary uptake. *Chemosphere* **100**, 97–104 (2014).
15. Mouneyrac, C. et al. Fate and effects of metal-based nanoparticles in two marine invertebrates, the bivalve mollusc *Scrobicularia plana* and the annelid polychaete *Hediste diversicolor*. *Environ. Sci. Pollut. Res.* **21**, 7899–7912 (2014).
16. García-Cambero, J. P. et al. Converging hazard assessment of gold nanoparticles to aquatic organisms. *Chemosphere* **93**, 1194–1200 (2013).
17. Bar-Ilan, O., Albrecht, R. M., Fako, V. E. & Furgeson, D. Y. Toxicity assessments of multisized gold and silver nanoparticles in zebrafish embryos. *Small* **5**, 1897–1910 (2009).
18. Hull, M. S. et al. Filter-feeding bivalves store and biodeposit colloidally stable gold nanoparticles. *Environ. Sci. Technol.* **45**, 6592–6599 (2011).
19. Renault, S. et al. Impacts of gold nanoparticle exposure on two freshwater species: a phytoplanktonic alga (*Scenedesmus subspicatus*) and a benthic bivalve (*Corbicula fluminea*). *Gold Bull.* **41**, 116–126 (2008).
20. Lee, B.-T. & Ranville, J. F. The effect of hardness on the stability of citrate-stabilized gold nanoparticles and their uptake by *Daphnia magna*. *J. Hazard. Mater.* **213–214**, 434–439 (2012).
21. Pourbaix, M. *Atlas of Electrochemical Equilibria in Aqueous Solutions* (Pergamon, New York, NY, 1966).
22. Reith, F., Lengke, M. F., Falconer, D., Craw, D. & Southam, G. The geomicrobiology of gold. *ISME J.* **1**, 567–584 (2007).
23. Rea, M. A., Zammit, C. M. & Reith, F. Bacterial biofilms on gold grains—implications for geomicrobial transformations of gold. *FEMS Microbiol. Ecol.* **92**, fiw082 (2016).
24. Southam, G., Lengke, M. F., Fairbrother, L. & Reith, F. The biogeochemistry of gold. *Elements* **5**, 303–307 (2009).
25. Unrine, J. M. et al. Evidence for bioavailability of Au nanoparticles from soil and biodistribution within earthworms (*Eisenia fetida*). *Environ. Sci. Technol.* **44**, 8308–8313 (2010).
26. Judy, J. D., Unrine, J. M. & Bertsch, P. M. Evidence for biomagnification of gold nanoparticles within a terrestrial food chain. *Environ. Sci. Technol.* **45**, 776–781 (2011).
27. Sabo-Attwood, T. et al. Uptake, distribution and toxicity of gold nanoparticles in tobacco (*Nicotiana xanthi*) seedlings. *Nanotoxicology* **6**, 353–360 (2012).
28. Dale, A. L. et al. Modeling nanomaterial environmental fate in aquatic systems. *Environ. Sci. Technol.* **49**, 2587–2593 (2015).
29. Garner, K. L., Suh, S. & Keller, A. A. Assessing the risk of engineered nanomaterials in the environment: development and application of the nanoFate model. *Environ. Sci. Technol.* **51**, 5541–5551 (2017).
30. Meesters, J. A., Koelmans, A. A., Quik, J. T., Hendriks, A. J. & van de Meent, D. Multimedia modeling of engineered nanoparticles with SimpleBox4nano: model definition and evaluation. *Environ. Sci. Technol.* **48**, 5726–5736 (2014).
31. Unrine, J. M., Colman, B. P., Bone, A. J., Gondikas, A. P. & Matson, C. W. Biotic and abiotic interactions in aquatic microcosms determine fate and toxicity of Ag nanoparticles. Part 1. Aggregation and dissolution. *Environ. Sci. Technol.* **46**, 6915–6924 (2012).
32. Schippers, A. & Sand, W. Bacterial leaching of metal sulfides proceeds by two indirect mechanisms via thiosulfate or via polysulfides and sulfur. *Appl. Environ. Microbiol.* **65**, 319–321 (1999).
33. Aylmore, M. G. & Muir, D. M. Thiosulfate leaching of gold—a review. *Miner. Eng.* **14**, 135–174 (2001).
34. Dzombak, D. A., Ghosh, R. S. & Wong-Chong, G. M. *Cyanide in Water and Soil: Chemistry, Risk, and Management* (CRC Press, Boca Raton, FL, 2005).
35. Reith, F. & McPhail, D. C. Effect of resident microbiota on the solubilization of gold in soil from the Tomakin Park Gold Mine, New South Wales, Australia. *Geochim. Cosmochim. Acta* **70**, 1421–1438 (2006).
36. Faramarzi, M. A. & Brandl, H. Formation of water-soluble metal cyanide complexes from solid minerals by *Pseudomonas plecoglossicida*. *FEMS Microbiol. Lett.* **259**, 47–52 (2006).
37. Brandl, H., Lehmann, S., Faramarzi, M. A. & Martinelli, D. Biomobilization of silver, gold, and platinum from solid waste materials by HCN^--forming microorganisms. *Hydrometallurgy* **94**, 14–17 (2008).
38. Fischer, J. M., Reed-Andersen, T., Klug, J. L. & Chalmers, A. G. Spatial pattern of localized disturbance along a southeastern salt marsh tidal creek. *Estuaries Coasts* **23**, 565–571 (2000).
39. Dhir, B., Sharmila, P. & Saradhi, P. P. Potential of aquatic macrophytes for removing contaminants from the environment. *Crit. Rev. Environ. Sci. Technol.* **39**, 754–781 (2009).
40. Sabater, S. et al. Monitoring the effect of chemicals on biological communities. The biofilm as an interface. *Anal. Bioanal. Chem.* **387**, 1425–1434 (2007).
41. Baudrimont, M. et al. Trophic transfer and effects of gold nanoparticles (AuNPs) in *Gammarus fossarum* from contaminated periphytic biofilm. *Environ. Sci. Pollut. Res.* **25**, 11181–11191 (2018).
42. Colman, B. P. et al. Emerging contaminant or an old toxin in disguise? Silver nanoparticle impacts on ecosystems. *Environ. Sci. Technol.* **48**, 5229–5236 (2014).
43. Nicol, M. J., Fleming, C. A. & Paul, R. L. in *The Extractive Metallurgy of Gold in South Africa* (ed Stanley, G. G.) Ch. 15 (South African Institute of Mining and Metallurgy, Johannesburg, 1987).
44. Glenn, J. B., White, S. A. & Klaine, S. J. Interactions of gold nanoparticles with freshwater aquatic macrophytes are size and species dependent. *Environ. Toxicol. Chem.* **31**, 194–201 (2012).
45. Marsden, J. & House, I. *The Chemistry of Gold Extraction* 2nd edn (SME, Littleton, CO, 2006).
46. Lewis, G. & Shaw, C. F. III Competition of thiols and cyanide for gold (I). *Inorg. Chem.* **25**, 58–62 (1986).
47. Mishra, A. & Malik, A. Recent advances in microbial metal bioaccumulation. *Crit. Rev. Environ. Sci. Technol.* **43**, 1162–1222 (2013).

48. Yee, N., Benning, L. G., Phoenix, V. R. & Ferris, F. G. Characterization of metal-cyanobacteria sorption reactions: a combined macroscopic and infrared spectroscopic investigation. *Environ. Sci. Technol.* **38**, 775–782 (2004).
49. Stolz, J. F., Oremland, R. S., Paster, B. J., Dewhirst, F. E. & Vandamme, P. in *Bergey's Manual of Systematics of Archaea and Bacteria* (eds Whitman, W. B. et al.) Ch. Sulfurospirillum (Wiley, New York, NY, 2015).
50. Zheng, S., Wang, B., Li, Y., Liu, F. & Wang, O. Electrochemically active iron (III)-reducing bacteria in coastal riverine sediments. *J. Basic Microbiol.* **57**, 1045–1054 (2017).
51. Milan, M. et al. Microbiota and environmental stress: how pollution affects microbial communities in Manila clams. *Aquat. Toxicol.* **194**, 195–207 (2018).
52. Ouyang, F., Ji, M., Zhai, H., Dong, Z. & Ye, L. Dynamics of the diversity and structure of the overall and nitrifying microbial community in activated sludge along gradient copper exposures. *Appl. Microbiol. Biotechnol.* **100**, 6881–6892 (2016).
53. Wasi, S., Tabrez, S. & Ahmad, M. Use of *Pseudomonas* spp. for the bioremediation of environmental pollutants: a review. *Environ. Monit. Assess.* **185**, 8147–8155 (2013).
54. Ebbs, S. Biological degradation of cyanide compounds. *Curr. Opin. Biotechnol.* **15**, 231–236 (2004).
55. Dubey, S. K. & Holmes, D. S. Biological cyanide destruction mediated by microorganisms. *World J. Microbiol. Biotechnol.* **11**, 257–265 (1995).
56. Yin, Y., Liu, J. & Jiang, G. Sunlight-induced reduction of ionic Ag and Au to metallic nanoparticles by dissolved organic matter. *ACS Nano* **6**, 7910–7919 (2012).
57. Đurović, M. D., Bugarčić, Ž. D., Heinemann, F. W. & Eldik, Rvan Substitution versus redox reactions of gold(III) complexes with L-cysteine, L-methionine and glutathione. *Dalton Trans.* **43**, 3911–3921 (2014).

Acknowledgements

The authors thank S. M. Anderson and B. P. Colman for their help setting up, monitoring and collecting samples during the experiment, S. Marinakos for providing TEM characterization of the Au-NPs, A. Curinier for insights and B. Perrotta for analyses of Au concentrations on mesocosm biofilms. This work was supported by the National Science Foundation (NSF) and the Environmental Protection Agency (EPA) under NSF Cooperative Agreement EF-0830093 and DBI-1266252, Center for the Environmental Implications of NanoTechnology (CEINT). Funds for graduate student summer support was supplied by the Duke Wetland Center Endowment. Portions of this work were performed at the Stanford Synchrotron Radiation Lightsource (SSRL) on beamline 11-2, a Department of Energy supported facility.

Author contributions

A.A., M.S., E.M., N.B., E.S.-S. and J.D.R. performed experiments and/or data analysis. A.A., M.S., E.S.B., N.K.G., M.R.W., J.M.U. and G.V.L. were involved in experimental design and writing. All authors discussed the results and commented on the manuscript.

Additional information

Supplementary information is available for this paper at https://doi.org/10.1038/s41565-018-0231-y.

Reprints and permissions information is available at www.nature.com/reprints.

Correspondence and requests for materials should be addressed to G.V.L.

Publisher's note: Springer Nature remains neutral with regard to jurisdictional claims in published maps and institutional affiliations.

Methods

Au-NP synthesis and characterization. The citrate-coated Au-NPs were synthesized as described previously[58]. Au-NPs were 11.9 ± 1.2 nm in diameter (based on TEM) in the stock suspension and had an average hydrodynamic diameter of 41.3 ± 3.3 nm in filtered (0.45 µm) mesocosm water over a large pH range. The Au-NPs had a negative zeta potential over a large pH range in the mesocosm water. The hydrodynamic diameter and zeta potential in filtered mesocosm water at pH 7 were 10.9 ± 1.5 nm and −14 ± 1.25 mV, respectively.

See Supplementary Fig. 2 for more details about Au-NP characterization. Dissolved Au (filtered with a 10 kDa membrane) in the stock solution was below the detection limit (1 µg l^{-1}).

Wetland mesocosm set-up, sample collection and biofilm extraction. A large wetland mesocosm experiment (dimensions: 3.66 × 1.22 × 0.81 m), located in Duke Forest (Durham, NC, United States) (Supplementary Fig. 1) was set up to study the long-term effects of chronic low-concentration Au-NP exposure on aquatic biota (plants, phytoplankton, fish, invertebrates and microorganisms), and to perform a comprehensive analysis of the fate and transport of Au-NPs in a realistic and complex environment. The mesocosms contained terrestrial and aquatic plants, fish, freshwater snails and clams, planktonic and benthic organisms from a local wetland. Each week for six months, three mesocosms were dosed with 1 l of water augmented with 20 mg of Au-NPs, just below the water surface of the mesocosms. The total water volume in the mesocosms fluctuated with rainfall, but averaged about 300 l. Thus, the added amount of nanoparticles each week resulted in a water column concentration of ~70 µg l^{-1}. Three control mesocosms were dosed weekly with the same volume of water without Au-NPs.

After six months of exposure, 35 shoots (20 cm each) of *E. densa* were harvested from both (1) control mesocosms ('naive mesocosm') and (2) mesocosms dosed weekly with Au-NPs ('pre-exposed mesocosms'). Because the experiment was designed to continue for nine months in total, we could not harvest all of the *E. densa* biomass from the mesocosm. Thus, the total biomass of *E. densa* after six months of growth in the mesocosms had to be estimated. To estimate the total biomass in the mesocosms at $t = 6$ months, we used the relationship between *E. densa* growth rate and *E. densa* total biomass in 18 mesocosms at the end of the experiment ($t = 9$ months) (see equation (6)). The *E. densa* growth rate was determined by harvesting the biomass colonizing a known small volume (three mesh columns of 0.0157 m^3 each) after 100 days. Note that these meshes were introduced 100 days before the plant harvest. The relationship between the measured *E. densa* biomass after nine months and its measured growth rate is given by

$$E.\ densa\ \text{dry biomass (g)} = 49.4 \times E.\ densa\ \text{growth rates (mg m}^{-3}\ \text{day}^{-1}) + 336.2 \quad (6)$$

This relation was then used to estimate the total biomass in the mesocoms after six months of the experiment based on the growth rate of *E. densa* during the 100 days before $t = 6$ months. The growth rate of *E. densa* after six months of experiment was 7.8 ± 2.9 mg m^{-3} day^{-1} in the naive mesocosms, and 7.7 ± 1.8 mg m^{-3} day^{-1} in the Au-NPs exposed mesocosms, representing 721 ± 144 and 717 ± 89 g of dry total biomass, respectively.

About 3 l of water was collected from the naive mesocosms. The pH of the water during the harvest was 8.49. This water was sterilized in an autoclave at 121 °C for 20 min in moist heat. After one day, large settled particles were removed from the water. This sterilized water was used for the biofilm purification and Au biodissolution experiment described in the following.

Ten *Egeria densa* shoots (7 cm each) were immediately frozen after harvest. Five were used for X-ray absorption spectroscopy (XAS) analysis to determine Au speciation, and five were used for total Au concentration analysis by inductively coupled plasma mass spectrometry (ICP–MS). To collect the *E. densa* biofilm for laboratory experiments, 25 additional *E. densa* plants (20 cm each) were collected from either the naive or pre-exposed mesocosms. These were added to 400 ml of the sterile mesocosm water, gently shaken for 2 min to collect the biofilm growing on the leaves and then the plants were removed. The biofilms were washed three times by centrifugation at 12,000*g* for 10 min and the pellet was resuspended in sterile control mesocosm water. The last washed pellet was resuspended to reach 130 g l^{-1} of biofilm (fresh mass), and was used as the final inocula of pre-exposed or naive biofilms. These wased inocula were immediatly frozen and used for subsequent DNA extraction and sequencing.

Concentration and speciation of Au associated with *E. densa*. Five *E. densa* shoots were dried at 105 °C for 48 h, ground, and acid digested using HNO_3:H_2O_2:HCl (6:3:2). After dilution, the total Au concentration was measured by ICP–MS (Agilent 7700). The absence of drift during the analysis was verified by measuring two Au standards (5 and 10 ppb, Cole-Parmer) every ten samples. The calculated MDL was 0.5 mg Au per kg of dry plants.

For the speciation measurements, five frozen *E. densa* were freeze-dried at −53 °C under a vacuum of 0.01 mbar, homogenized, pressed into 5 mm pellets, sealed into Kapton tape, and stored under an anoxic atmosphere before analysis. Reference compounds used were gold cyanide (Au(I)–CN, molar ratio Au^0:NaCN 1:4 in deionized water) and gold cysteine (Au(I)–SH, $HAuCl_4$:L-cystein, 1:1 in 0.02 M NaCl[57]) synthesized and analysed as liquid samples, while gold nanoparticles (Au^0), gold hydroxide (Au(III)–OH), gold acetate (Au(III)–OAc) and gold chloride (Au(I)–Cl)) were purchased from Sigma Aldrich as dry powder, diluted in sugar and pressed into 5 mm pellets.

XANES spectra were collected using a liquid-nitrogen cryostat at the Au–L_{III} edge (11,918 eV) in fluorescence mode using a 100-element Ge detector at Stanford Synchrotron Radiation Light Source (SSRL) on beamline 11-2. Spectra were energy calibrated using an Au metal foil collected simultaneously with the sample spectra. Three to six individual spectra were acquired per pellet to obtain representative spectra. To minimize the risk of beam damage, each spectrum was collected at a different pellet location. The spectra were then averaged and normalized using SIXpack data processing software, and linear combination fitting was realized using Athena software.

Laboratory incubations to assess Au-NP biodissolution by biofilms. The two biofilm inocula (naive or pre-exposed) were diluted to 130 mg l^{-1} (fresh weight) in 30 ml of sterile control mesocosm water in glass vials covered with ethanol and UV sterilized parafilm to allow for gas exchange. They were incubated in the dark, at 25 °C, 150 r.p.m. for 2 days. After this incubation period, the biofilms were exposed to 70 µg l^{-1} of Au-NPs, or were unamended (biotic control) to ensure the absence of Au in the undosed samples. Abiotic controls with Au-NPs in sterile control mesocosm water were also prepared to test for the potential for abiotic dissolution of Au-NPs. All treatments were replicated four times and incubated in the dark, at 25 °C, 150 r.p.m. for two weeks.

During the 14 day dissolution experiment, 2 ml subsamples of the solution containing the biofilms were monitored for pH, and for total and dissolved Au concentration (defined as Au passing through a 10 kDa membrane; Amicon, Millipore, tested recovery with a gold-cyanide solution was 98%). The filtrate used to determine the dissolved Au fraction was acidified to 2% HCl and 6% HNO_3. The unfiltered solution used to determine the total Au fraction was digested using HNO_3:HCl 3:1 and diluted to 2% HCl and 6% HNO_3.

After the 14 day exposure, subsamples of the solutions were immediately frozen. These samples were used for $Au(CN)_2^-$ analysis, or free cyanide measurements.

Biofilm characterization, biomass and composition. DNA extraction of the two biofilm inocula was performed using a Biofilm DNA Isolation Kit (Mo Bio Laboratories). DNA concentration was measured using a Qubit dsDNA BR assay kit and a Qubit 2.0 fluorometer (Invitrogen) following the manufacturer's instructions. The DNA samples were shipped in 96-well plates to the sequencing facility at RTSF Michigan State University. We performed metagenomic DNA sequencing on an Illumina MiSeq sequencer with V2 chemistry to characterize the microbial community structure and composition. The bacterial community composition was determined by targeting the 16S rRNA gene (V4 region, primers 515f/806r). The sequences obtained were demultiplexed, trimmed, screened for chimaeras and clustered in OTUs at a 97% similarity threshold using the Qiime pipeline[59]. Taxonomic identification of the bacterial representative sequences was performed with the SILVA 128 database. For downstream community structure analysis, datasets were rarefied at the lowest sequencing depth: 12,266 sequences per sample.

To assess the biofilm growth over the 14 days of experiment, we measured the dry biomass present in subsamples taken from the solutions. The subsamples were filtered using a 0.45 µm filter that had been pre-dried at 100 °C for 24 h and pre-weighed. A 4 ml volume of each sample was collected and filtered under sterile conditions. The filters were dried at 100 °C over night, and weighed again to assess the dry biomass of the biofilm during incubation.

Cyanide ion and Au–cyanide complex measurements. The presence of cyanide ion in the dissolved fraction of the samples and the presence of Au–cyanide complexes in the total samples were determined. The free cyanide concentration was quantified with a cyanide-ion-selective electrode (Orion cyanide electrode, Thermo Scientific). This measurement was conducted in a fume hood to avoid potential exposure to volatile and toxic HCN. All of the standards (NaCN) used for the calibration curve, as well as the samples, were stabilized with alkaline ionic strength and pH adjustor solution (Orion, Thermo Scientific) so that the solution pH was >11 to dissociate HCN into CN^-, and the ionic strength was constant.

Detection of $Au(CN)_2^-$ was determined using a modified version of a method described previously[60]. The samples were filtered with glass-bed filters (0.22 µm) and analysed on an LC–MS/MS (liquid chromatography triple quadrupole mass spectrometry, Agilent 6430, Agilent 1100 Series). A 10 µl volume of sample was injected through a C18 column (Agilent Eclipse EBD-C18, 5 µM 4.6 × 150 mm), delivered using a 1:1 isocratic mixture of H_2O (18 MΩ cm, Millipore):methanol at a flow rate of 0.2 ml min^{-1}. The MS was run in negative polarity mode scanning (MS2 Scan) with a fragmentor energy of 80 V and cell accelerator voltage of 7 V. Nitrogen was used as the sheath gas. Masses (m/z) between 20 and 500 were scanned. The detection of $Au(CN)_2^-$ was performed via extracted ion chromatography (EIC) for ions that eluted between 6 and 11 min after injection and monitoring the spectrogram for peaks at m/z 249 using Agilent MassHunter Qualitative Analysis Worskstation Software peak selection.

Statistical analysis. The effects of the inoculum type (naive or pre-exposed) and of Au-NP exposure (control or Au-NPs) on Au-NP dissolution potential and biofilm biomass each day were tested using a two-way ANOVA followed by Tukey's HSD post hoc tests. The normality and homoscedasticity of the data were checked before conducting analyses. The similarity between the bacterial composition of the different samples was calculated using Bray–Curtis distances with the *vegdist* function of the Vegan package in R software (3.2.3 Version).

Data availability. The data that support the plots within this paper and other findings of this study are available from the corresponding author upon reasonable request.

References

58. Turkevich, J., Stevenson, P. C. & Hillier, J. A study of the nucleation and growth processes in the synthesis of colloidal gold. *Discuss. Faraday Soc.* **11**, 55–75 (1951).
59. Caporaso, J. G. et al. QIIME allows analysis of high-throughput community sequencing data. *Nat. Methods* **7**, 335–336 (2010).
60. Minakata, K., Nozawa, H., Gonmori, K., Suzuki, M. & Suzuki, O. Determination of cyanide, in urine and gastric content, by electrospray ionization tandem mass spectrometry after direct flow injection of dicyanogold. *Anal. Chim. Acta* **651**, 81–84 (2009).